Supplementary information

S1) Interposer process flow

The process flow of the interposer front-side fabrication is schematically described in Figure S1.

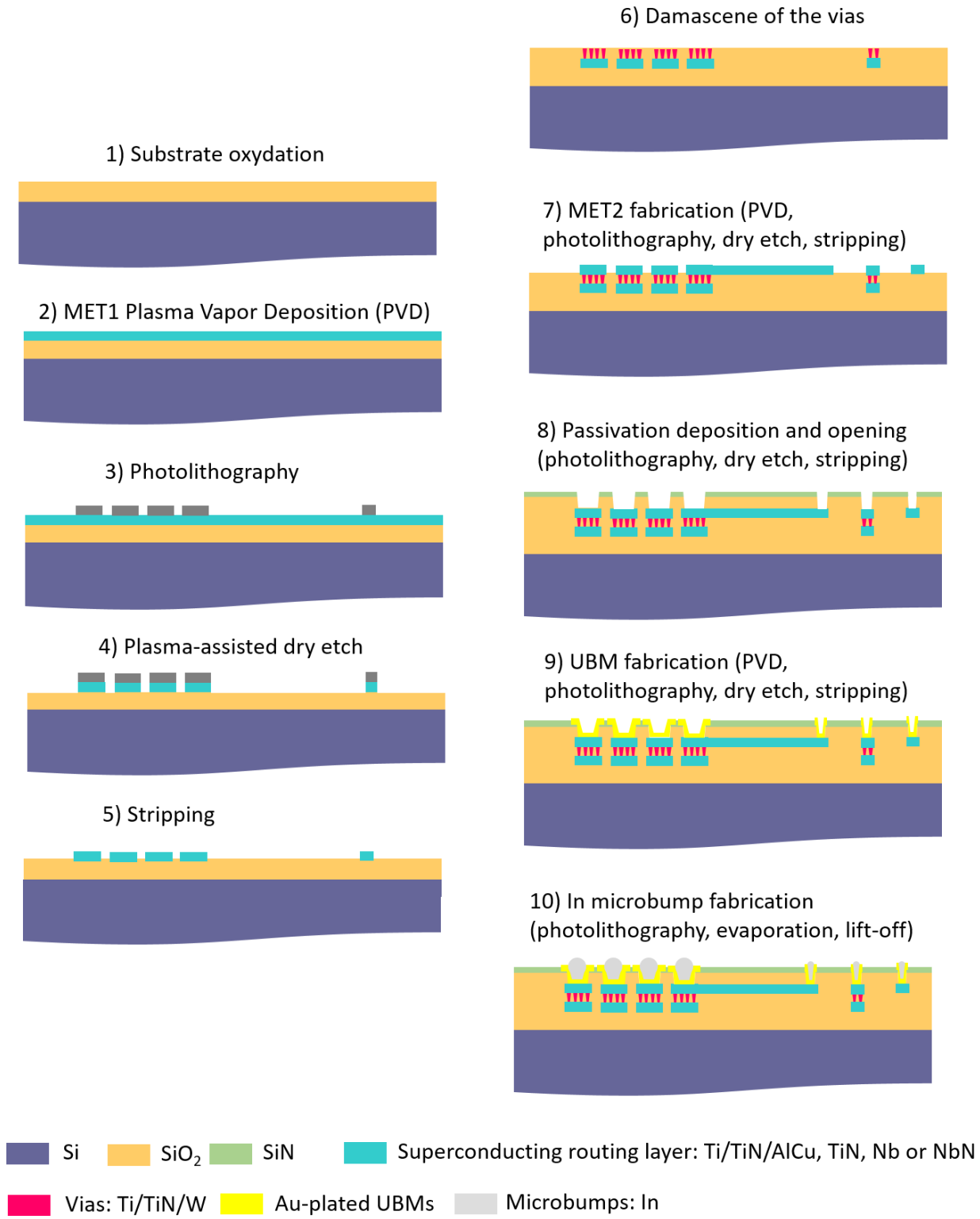

Figure S1- Schematic representation of the complete front-side process flow of the interposer.

S2) Fabrication and morphological characterizations of the Nb and NbN routing levels

Different materials and stack layers have been used in this study to form MET1 and MET2 superconducting layers. MET1 layer has mostly been made from a standard Ti/TiN/AlCu stack, while MET2 layer can integrate the same stack or more attractive superconductors such as TiN, Nb or NbN. While the fabrication of Ti/TiN/AlCu and TiN tracks use mature recipes developed for years for microelectronics, engineering studies were needed to develop proper etching conditions for Nb and NbN with CF_4 as primary ion etching gas. Figure S2 and Figure S3 display morphological characterizations of Nb and NbN tracks, respectively, using best-developed etch and stripping processes so far. A slight over-etching (tens of nm) of the SiO_2 template, that is yet to optimize, is observed for both cases on Figure S2(e) and Figure S3(e). Nonetheless, the roughness of the SiO_2 and the superconductor (< 3nm) are not impacted by the etching and stripping steps.

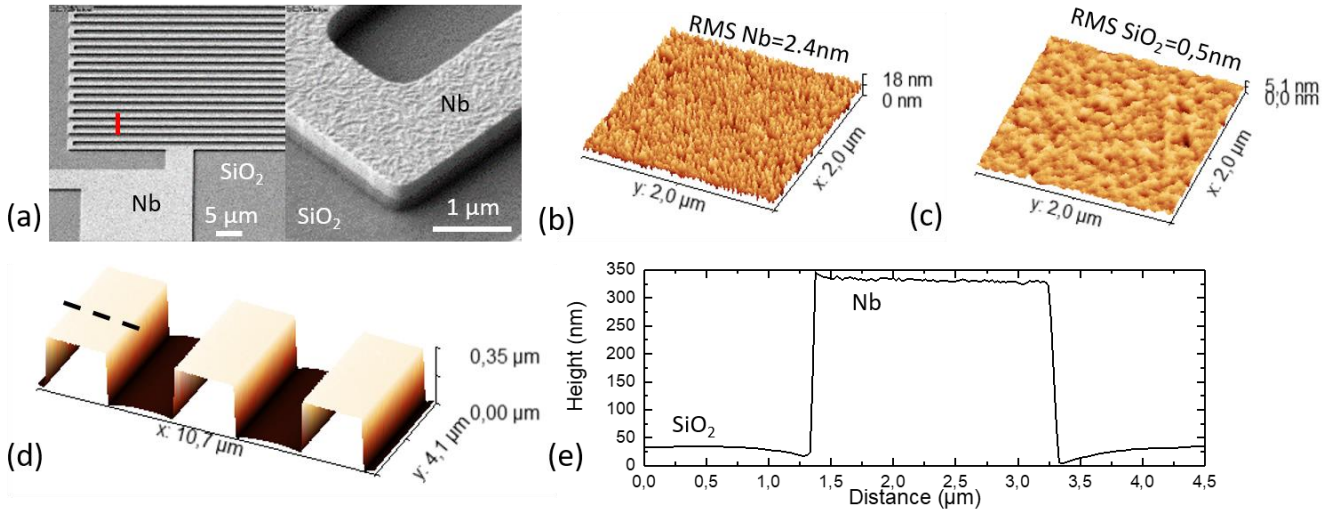

Figure S2- Morphological characterizations of Nb routing tracks. (a) Scanning electron micrographs of the Nb tracks just after etching. (b) and (c) 2x2 µm² atomic force micrographs on the Nb and SiO_2, respectively. (d) 3D map of the tracks of (a), taken along the red line. (e) 1D profile extracted along the black dashed line of (d).

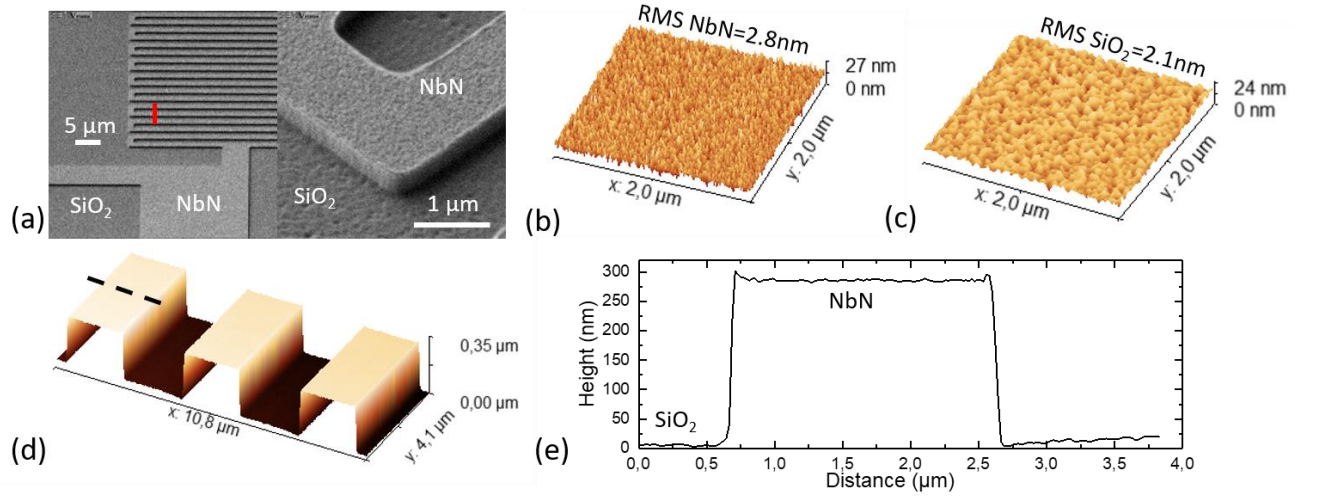

Figure S3- Morphological characterizations of NbN routing tracks. (a) Scanning electron micrographs of the NbN tracks just after etching. (b) and (c) 2x2 µm² atomic force micrographs on the NbN and SiO_2, respectively. (d) 3D map of the tracks of (a), taken along the red line. (e) 1D profile extracted along the black dashed line of (d).

S3) Electrical characterizations of superconducting routing levels

S3a) Impact of the integration steps on *Rsq*, T_c and *RRR*

Wafer-level parametric tests have been performed at 300 K along the process to evaluate the impact of each integration steps (MET2 patterning, passivation deposition and UBM fabrication) on the routing layer electrical properties. Figure S4 displays the cumulative percentage of the sheet resistances along the wafers for Ti/TiN/AlCu, TiN, Nb and NbN layers. TiN integration appears robust with no resistance variation along the process and a sheet resistance value of 3.35 +/- 0.10 Ω/sq (see Figure S4 (b)). Concerning Ti/TiN/AlCu routing, a slight increase of about 3% of the sheet resistance, from 0.069 +/- 0.003 Ω/sq to 0.071 +/- 0.003 Ω/sq, is noticed after the passivation of the metal. This is attributed to the formation of Al_3Ti intermetallic when the substrate reaches 400°C for the passivation deposition [1]. The resistance is not impacted further by the UBM fabrication for which the thermal budget is much lower.

Similar behavior is observed for NbN on Figure S4(d) with a 7% increase of the resistance from 20.0 +/- 0.7 Ω/sq to 21.5 +/- 0.8 Ω/sq after the passivation and UBM fabrication. Effects of the integration steps are mostly observed in the case of Nb as can be seen in Figure S4 (c). An increase of about 30 %, from 1.07 +/- 0.04 Ω/sq to 1.55 +/- 0.06 Ω/sq, of the resistance is measured after passivating the metal. The insulating oxide Nb_2O_5 is likely to form at the interface between Nb and SiO_2 increasing the resistance of the lines [2]. The fabrication of the UBM is accompanied by a reduction of the resistance (~ -10%) down to 1.39 +/- 0.06 Ω/sq. A more detailed study, including TEM imaging, would be needed to properly understand the modification of Nb film and its properties during the integration.

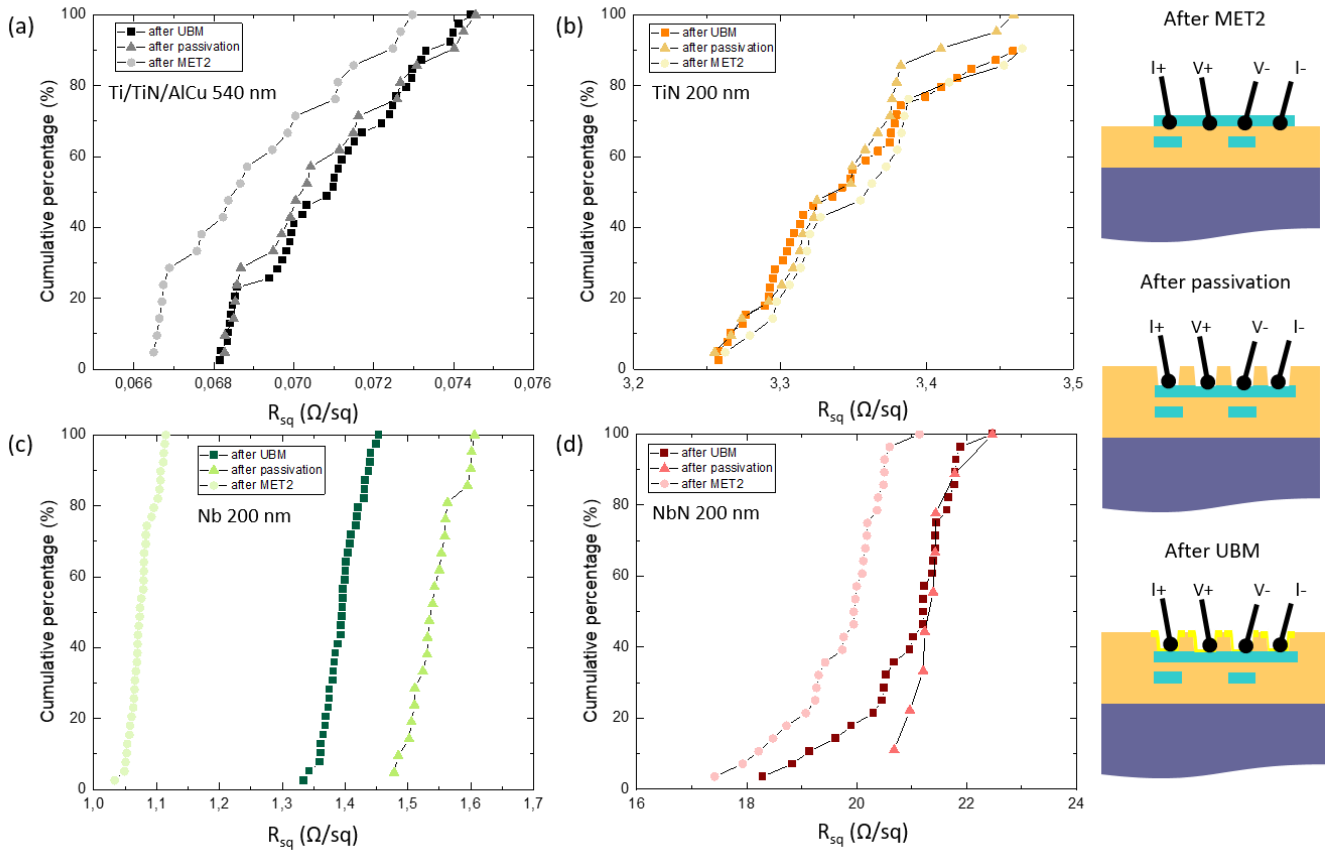

Figure S4- 300 K parametric test results for (a) Ti/TiN/AlCu, (b) TiN, (c) Nb and (d) NbN routing layers. Each panel shows data obtained after MET2 integration step, after passivation deposition and after the UBM fabrication.

Figure S5 presents the evolution of R_{sq} as a function of the temperature between 300 K and 2 K for TiN, Nb and NbN routing at the different integration steps. As shown on Figure S5 (a) and (c), passivation and UBM integraton steps have no impact on

the resistance evolution with temperature and so on the *RRR* for TiN and NbN. The critical temperature is also unchanged. The situation is different for Nb. At 300 K, consistently with the parametric tests discussed just before, one can already see an increase of R_{sq} after passivation followed by a decrease of 10% after UBM step. The difference of R_{sq} at low temperatures are also significant leading to the following *RRR* variations: 9.5 after MET2 patterning, 2.3 after depositing the passivation and 2.5 after fabricating the UBM. The reduction of the *RRR* by a factor of about 3 and the increase of R_{sq} values after passivation suggest an increase of the disorder in the Nb routing layer. This could be attributed to a significant oxidation during the process and by the interdiffusion with the SiO_2 layer on top. The critical temperature is also affected with a reduction from 9.3 K to 7.7 K. Technological solutions (not discussed here) are currently investigated to protect the Nb layers from oxidation and from intermixing with SiO_2 passivation layer during the integration, to optimize the properties of this routing option.

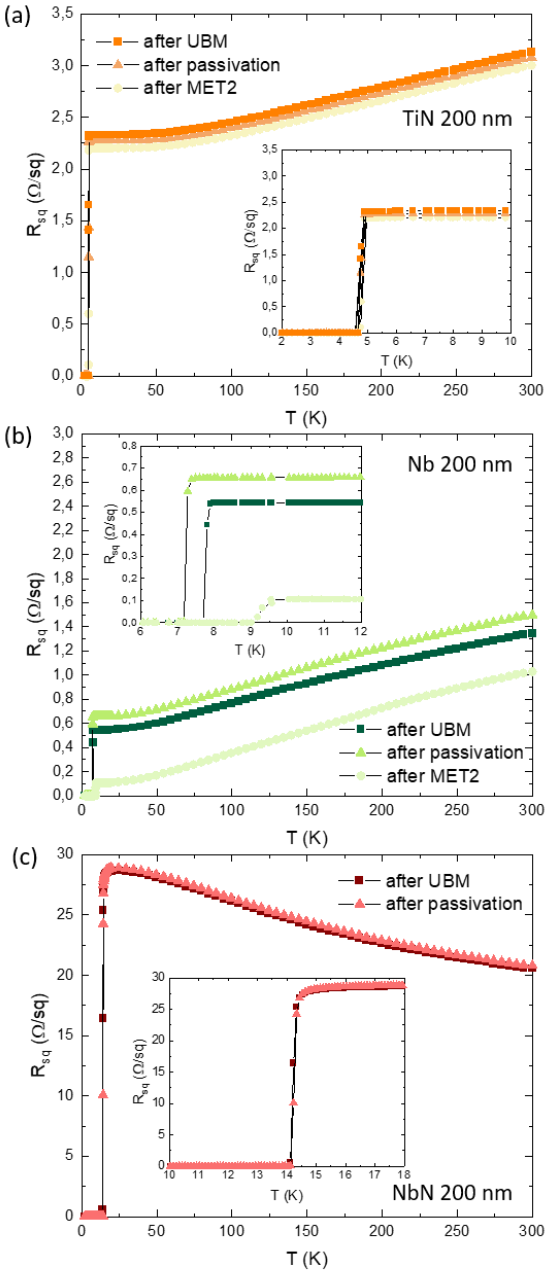

Figure S5- R_{sq} as a function of *T* between 300 K and 2 K for (a) TiN, (b) Nb and (c) NbN after the realization of MET2 level, after the passivation deposition and opening and after the UBM fabrication. Insets focus on R_{sq} variations at low temperatures to highlight the superconducting transitions.

S3b) Extraction of the critical magnetic field

Resistance measurements as a function of the temperature were repeated for several values of the static perpendicular magnetic field B for the different routing materials as displayed in Figure S6 for NbN, Figure S7 for Nb, Figure S8 for TiN and in Figure S9 for Ti/TiN/AlCu routing layers. The extraction of the critical temperature at each magnetic field is reported in the panels (b), showing a linear correlation between T_c and B. The linear extrapolation of the data is used to estimate the critical field value $B_{c2}(0K)$ for each routing materials based on $\xi(T) = \frac{\xi(0)}{\sqrt{1-\frac{T}{T_C}}}$ and $B_{c2}(T) = \frac{\Phi_0}{2\pi\xi^2(T)}$ [3].

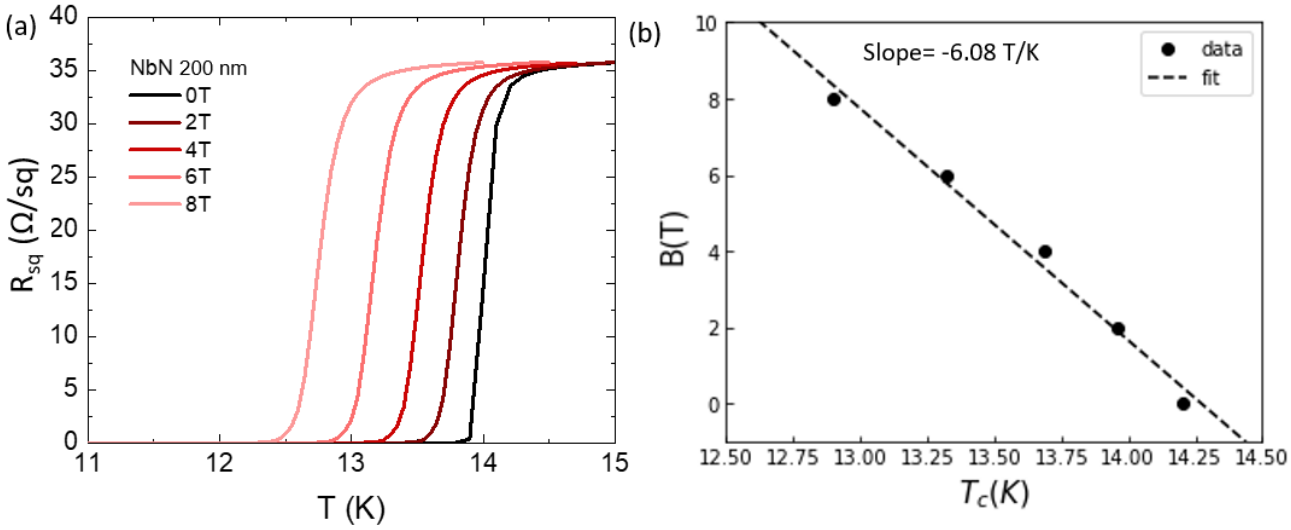

Figure S6-(a) Sheet resistance R_{sq} as a function of the temperature for different magnetic field B values in between 0 T and 8 T for 200 nm-thick NbN routing layer. (b) Evolution of the critical temperature T_c as a function of B and the associated linear fit.

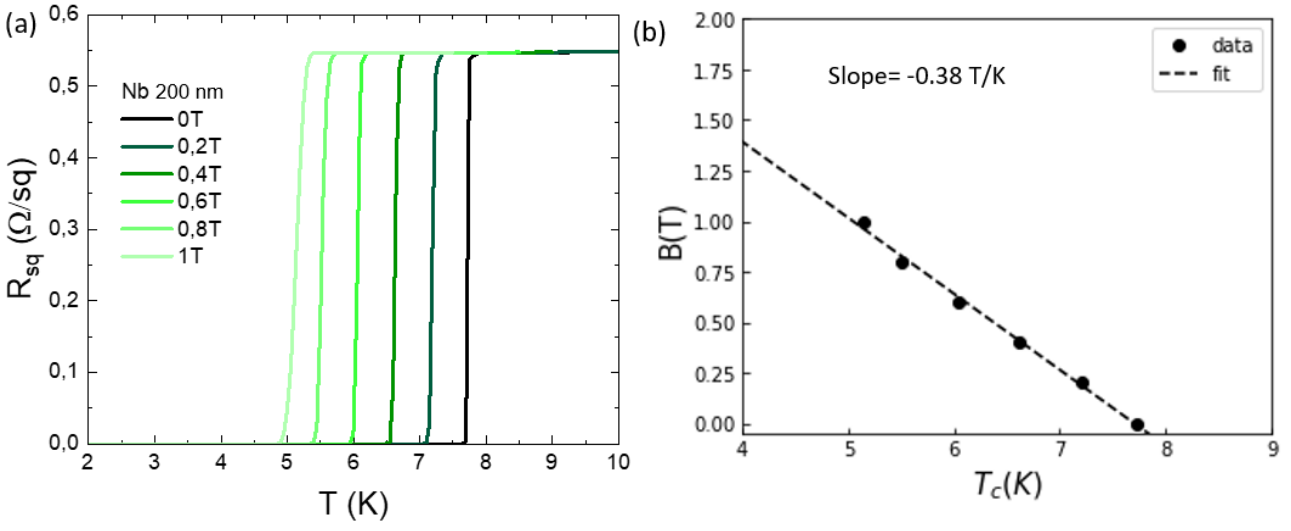

Figure S7-(a) Sheet resistance R_{sq} as a function of the temperature for different magnetic field B values in between 0 T and 1 T for 200 nm-thick Nb routing layer. (b) Evolution of the critical temperature T_c as a function of B and the associated linear fit.

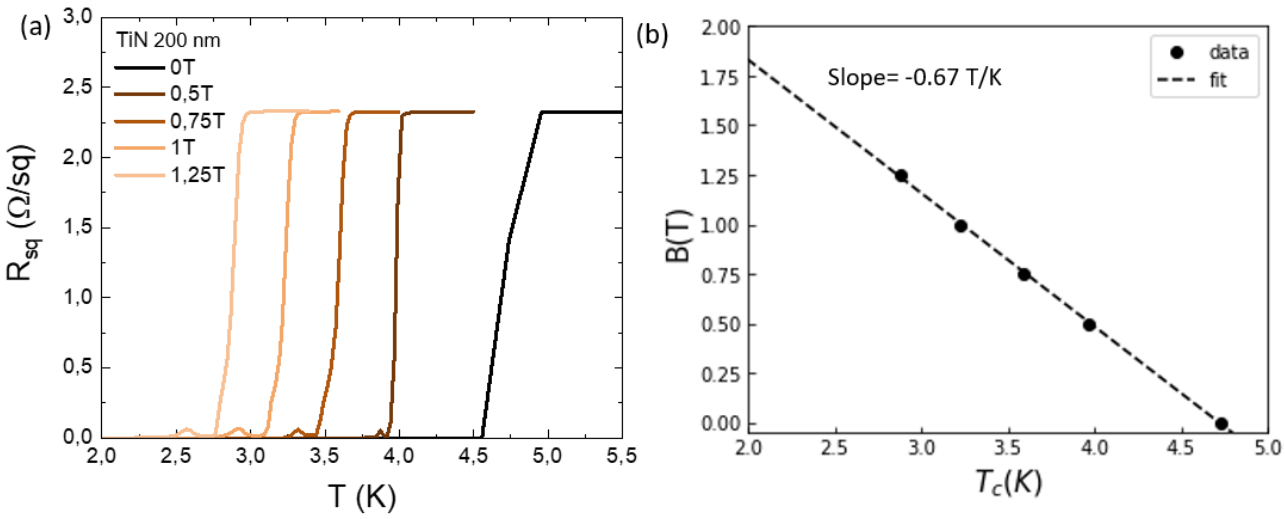

Figure S8-(a) Sheet resistance R_{sq} as a function of the temperature for different magnetic field B values in between 0 T and 1.25 T for 200 nm-thick TiN routing layer. (b) Evolution of the critical temperature T_c as a function of B and the associated linear fit.

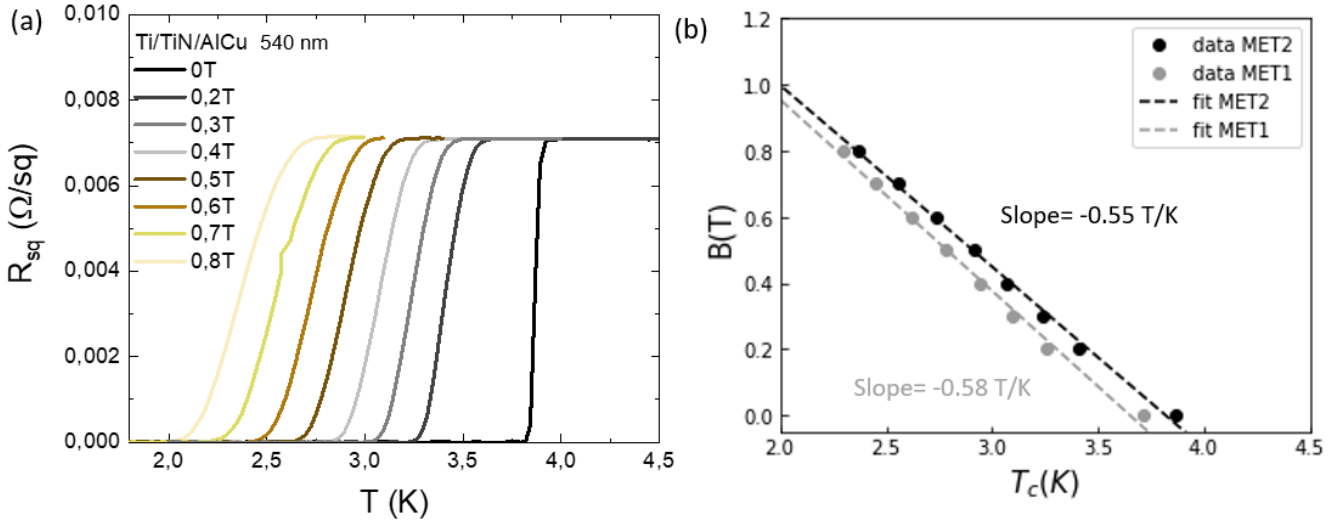

Figure S9-(a) Sheet resistance R_{sq} as a function of the temperature for different magnetic field B values in between 0 T and 0.8 T for 540 nm-thick Ti/TiN/AlCu routing layer on MET2 integration level. (b) Evolution of the critical temperature T_c as a function of B and the associated linear fit.

S3c) Extraction of the critical current

Figure S10 (a), Figure S11 (a) and Figure S12 (a) present I-V measurements performed on a 25 µm wide NbN channel at T=13 K, on a 2 µm wide Nb channel at 6.5 K and on a 6 µm wide TiN channel at 3.5 K, respectively. The width of the channel was chosen to limit the resistance value in the order of hundreds of Ohm for these measurements. For each material, the excitation current I_{ex} was swept from 0 mA to a positive value and then swept back to 0 mA (data not shown here) after reaching the superconductor-normal transition. The critical current I_c value corresponds to the I_{ex} value at which the voltage abruptly switches to a non-zero value. These measurements were done for several temperatures close to T_c and for different magnetic

fields, 0T, 0.01T and 0.1T, perpendicular to the sample. Note that the gain limits in the PPMS cryostat prevented from doing I-V measurements for which I_{ex} exceeded ~20 mA, preventing measurements at $T/T_c << 1$. Each measurement was repeated four times with a very small dispersion of I_c as denoted by the barely visible error bars in Figure S10 (b). I_c experimental values are plotted as a function of T/T_c in Figure S10(b), Figure S11(b) and Figure S12(b) for NbN, Nb and TiN channels, respectively. These experimental data are fitted using Ginzburg-Landau theory to estimate the critical current $I_c^{GL}(0\ K)$. As explained in the main text, we then consider $I_c(0\ K) = I_c^{GL}(0\ K)/2$ [4].

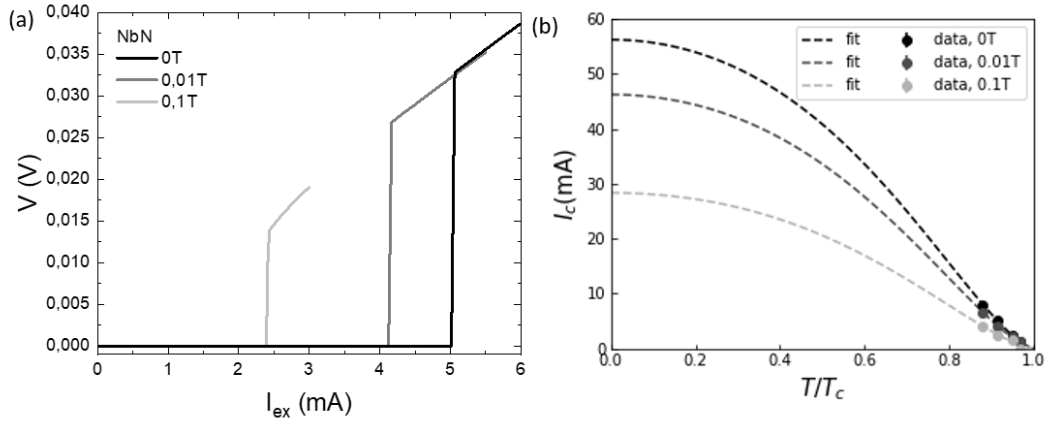

Figure S10- (a) V-I curves obtained at 0T, 0.01T and 0.1T at T=13 K for a 200 nm-thick NbN routing layer. (b) Evolution of the measured critical current I_c as a function of T/T_c at 0T, 0.01T and 0.1T and the associated fits of I_c^{GL} using Ginzburg-Landau model.

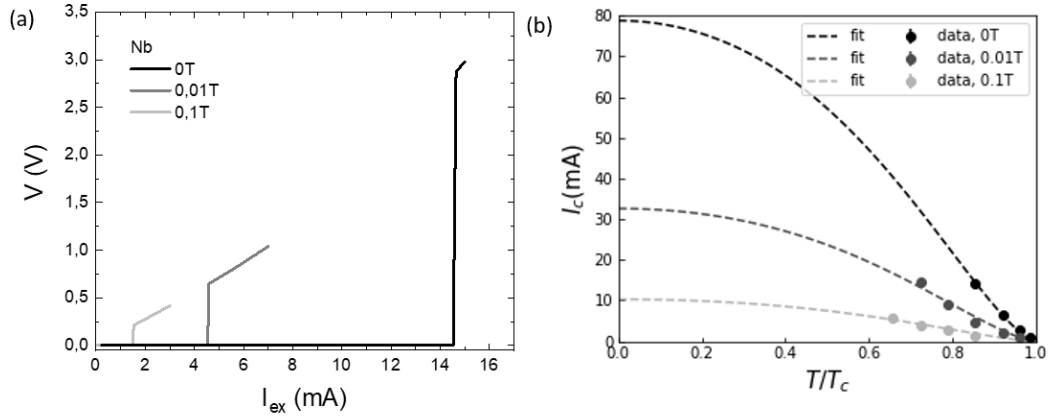

Figure S11- (a) V-I curves obtained at 0T, 0.01T and 0.1T at T=6.5 K for a 200 nm-thick Nb routing layer. (b) Evolution of the measured critical current I_c as a function of T/T_c at 0T, 0.01T and 0.1T and the associated fits of I_c^{GL} using Ginzburg-Landau model.

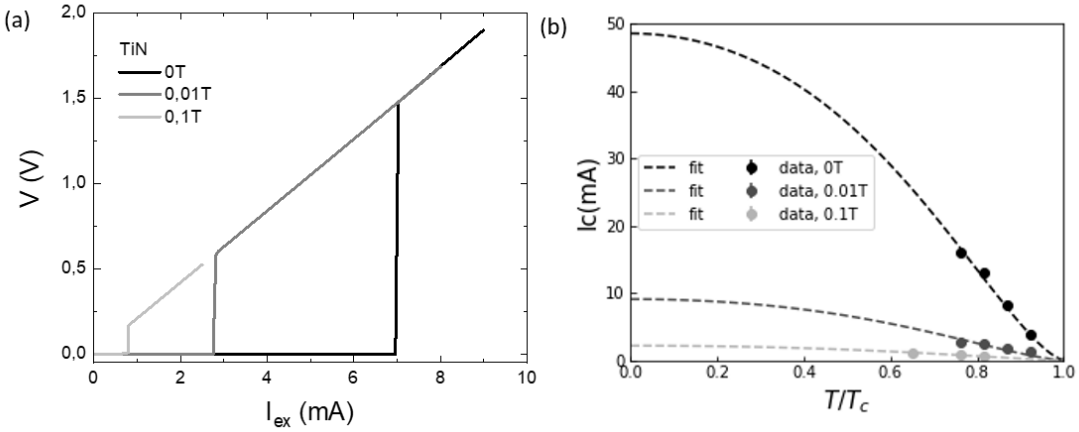

Figure S12- (a) V-I curves obtained at 0T, 0.01T and 0.1T at T=3.5 K for a 200 nm-thick TiN routing layer. (b) Evolution of the measured critical current I_c as a function of T/T_c at 0T, 0.01T and 0.1T and the associated fits of I_c^{GL} using Ginzburg-Landau model.

Similar measurements were performed on Ti/TiN/AlCu as displayed in Figure S13. This time, the I-V curve shape does not show an abrupt transition from 0 to a positive voltage but a smooth increase of the voltage with I_{ex}. The presence of two superconductors TiN and AlCu in the stack layer might explain this behavior. To extract I_c from these curves, a 1 µV criterion was used.

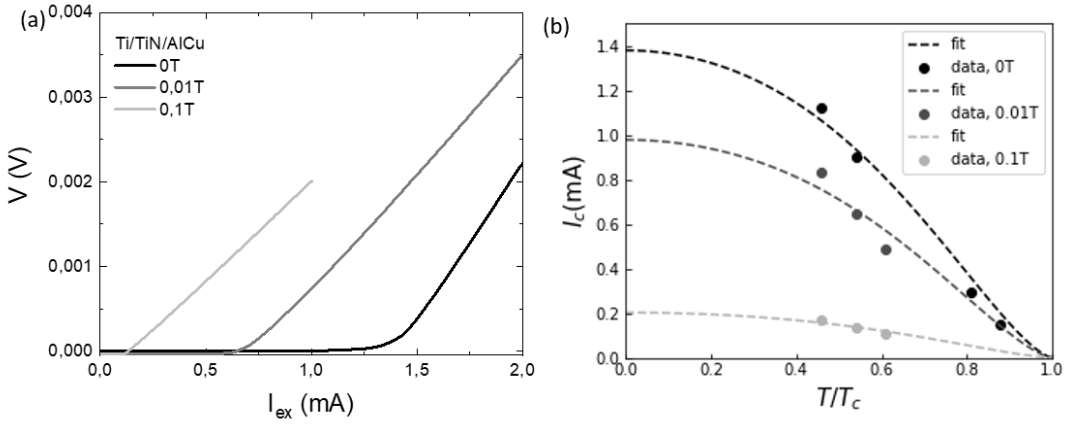

Figure S13- (a) V-I curves obtained at 0T, 0.01T and 0.1T at T=2 K for a 540 nm-thick Ti/TiN/AlCu routing layer integrated on MET1 level. (b) Evolution of the measured critical current I_c as a function of T/T_c at 0T, 0.01T and 0.1T and the associated fits of I_c^{GL} using Ginzburg-Landau model.

S4) Electrical characterizations of MET1-MET2 chain

The electrical characterizations presented in the main text focus on a single layer. Here we show additional data obtained on a chain connecting 2 µm-wide MET1 and MET2 sections. MET2 is made from Ti/TiN/AlCu, TiN, Nb or NbN layers and MET1 from Ti/TiN/AlCu. Four Ti/TiN/W vias are used at each connection between MET1 and MET2 layers. Figure S14 presents the link resistance values obtained on chains made with 7000 links between MET1 and MET2 layers. The link resistance is obtained by dividing the total resistance of the chain by the number of links. These parametric tests have been performed at 300 K on an automated probing station. One can first notice that the measurement yield is larger than 95% on the 200 mm wafers for all the probed chains, highlighting the proper electrical contact between MET1 layer, the vias and MET2 layer no matter which

superconductor was integrated as MET2. The dispersion observed when MET2 is made of Ti/TiN/AlCu, TiN and Nb is mostly explained by slight resistance variations or defects at the wafer edges that affect either MET1 level, the vias or MET2 level, depending on the tested dies.

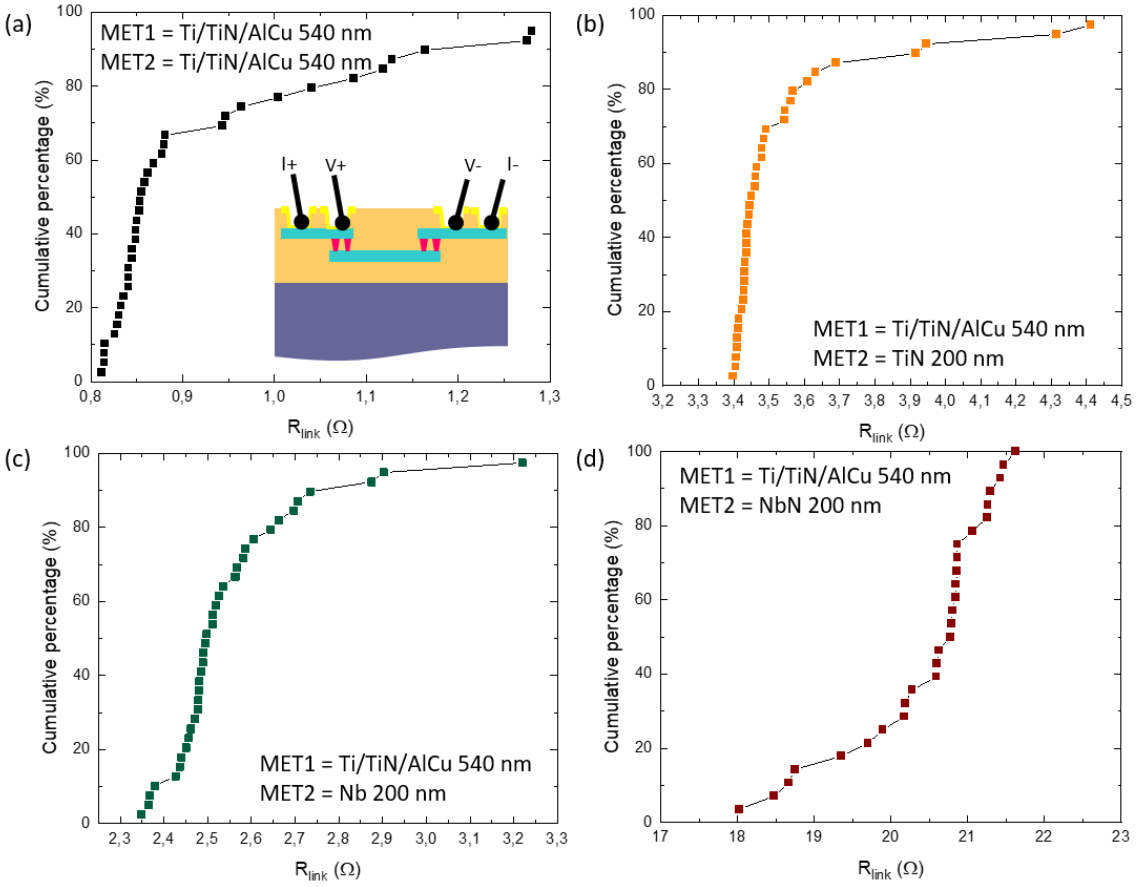

Figure S14- Cumulative % as a function of the link resistance R_{link} for chains made of MET1 layer in Ti/TiN/AlCu and MET2 layer in (a) Ti/TiN/AlCu, (b) TiN, (c) Nb and (d) NbN. Inset of (a) represents the measurement configuration.

Complementary to these parametric tests, Figure S15 presents the evolution of the link resistance as a function of the temperature, between 300 K and 2 K, in the case where the chain includes NbN on MET2. In the normal state, one can see that the resistance varies similarly to a single layer of NbN (see Figure S5 (c)) due to the large difference (a factor of about 300) of R_{sq} existing between NbN on MET2 and Ti/TiN/AlCu on MET1. At low temperatures, two transitions are observed (see the black arrows in the inset of Figure S15): a sharp one at 14 K corresponding to NbN superconducting-normal transition on MET2 and a smoother one at around 3.6 K attributed to Ti/TiN/AlCu transition on MET1. The sharpness of the transitions is explained by difference of sheet resistance existing between the chain blocks. For lower temperatures, the resistance value corresponds to the four Ti/TiN/W vias connecting the layers. It linearly decreases down to 2 K. Additional measurements at lower temperatures would be needed to fully characterize this chain at the operating temperature of spin qubits.

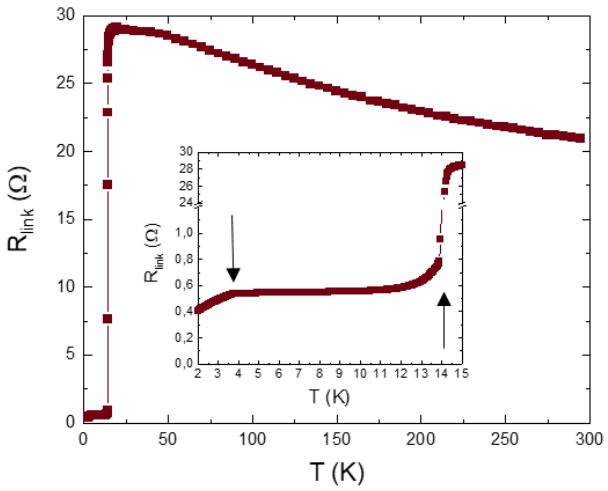

Figure S15-Link resistance R_{link} as a function of the temperature T for a chain made with MET1 in Ti/TiN/AlCu, Ti/TiN/W vias and MET2 in NbN. The inset shows a zoom at low temperatures.

S5) Optical micrographs of the inductors

The fabricated single layer inductors Ind A, Ind B and Ind C are visible in Figure S16.

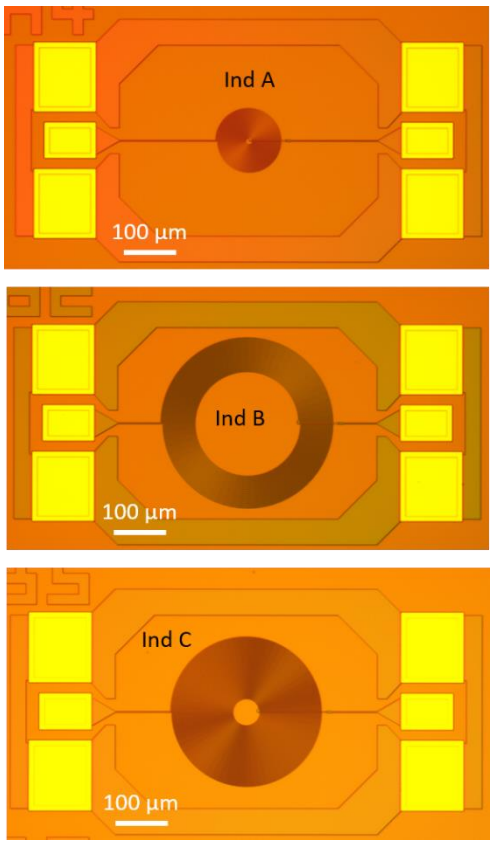

Figure S16 - Optical micrographs of Ind A, Ind B ad Ind C.

References

[1] H. Onoda, T. Narita and K. Hashimoto, “Interfacial Reactions in Al-Alloy/Ti/Silicon-Dioxide-Based Substrate Structures for Multilayered Interconnects”, Jpn. J. Appl. Phys., 34, 4728-4735, (1995).

[2] M.D. Henry, S. Wolfley, T. Young, T. Monson, C.J. Pearce, R. Lewis, B. Clark, L. Brunke and N. Missert, “Degradation of Superconducting Nb/NbN Films by Atmospheric Oxidation”, IEEE Transactions on Applied Superconductivity, 27, 1100505, (2017).

[3] E. Helfand and N.R. Werthamer, “Temperature and Purity Dependence of the Superconducting Critical Field, H_{c2}. II”, Physical Review, 147, 288-294, (1966).

[4] A. Engel, H. Bartolf, A. Schilling, K. Il’in, M. Siegel, A. Semenov and H-W. Hubers, “Temperature- and field-dependence of critical currents in NbN microbridges”, Journal of Physics: Conference Series 97, 012152, (2008).